

Quantum cosmology of a Hořava-Lifshitz model coupled to radiation

G. Oliveira-Neto and L. G. Martins

Departamento de Física,
Instituto de Ciências Exatas,
Universidade Federal de Juiz de Fora,
CEP 36036-330 - Juiz de Fora, MG, Brazil.
gilneto@fisica.ufjf.br, laysamartinsymail@yahoo.com.br

G. A. Monerat

Departamento de Modelagem Computacional,
Instituto Politécnico do Rio de Janeiro,
Universidade do Estado do Rio de Janeiro,
Rua Bonfim, 25 - Vila Amélia - Cep 28.625-570,
Nova Friburgo, RJ, Brazil.
monerat@uerj.br

E. V. Corrêa Silva

Departamento de Matemática, Física e Computação,
Faculdade de Tecnologia,
Universidade do Estado do Rio de Janeiro,
Rodovia Presidente Dutra, Km 298, Pólo Industrial,
CEP 27537-000, Resende-RJ, Brazil.
evasquez@uerj.br

December 15, 2024

Abstract

In the present paper, we canonically quantize an homogeneous and isotropic Hořava-Lifshitz cosmological model, with constant positive spatial sections and coupled to radiation. We consider the projectable version of that gravitational theory without the detailed balance condition. We use the ADM formalism to write the gravitational hamiltonian of the model and the Schutz variational formalism to write the perfect fluid hamiltonian. We find the Wheeler-DeWitt equation for the model. That equation depends on several parameters. We study the case where the values of the parameters are chosen, such that, the solutions to the Wheeler-DeWitt equation are bounded. Initially, we solve it using the *Many Worlds* interpretation. Using wavepackets computed with the solutions to the Wheeler-DeWitt equation, we obtain the scalar factor expected value $\langle a \rangle$. We show that this quantity oscillate between maxima and minima values and never go to zero. That result gives an indication that the model is free from singularities, at the quantum level. We improve this result by showing that if we subtract a standard deviation of a from $\langle a \rangle$, this quantity is still positive. Then, we use the *DeBroglie-Bohm* interpretation. We compute the Bohm's trajectories for the scale factor and show that it never goes to zero. We show that each trajectory agrees with the corresponding $\langle a \rangle$. We also compute the quantum potential. That quantity helps understanding why the scale factor never vanishes.

1 Introduction

General relativity is presently the most successful theory of gravity, because it explains in a precise way several observational phenomenas and also predicts several new ones, that have been confirmed over the years. The most recent one was the first detection of gravitational waves [1]. The application of general relativity to cosmology gave rise to a very complete and detailed description of the birth and evolution of the Universe. Unfortunately, general relativity is not free of problems. In a series of theorems it was shown that, for very general and reasonable conditions, a large class of spacetimes which satisfy the general relativity field equations develop singularities [2]. Those singularities develop under extreme gravitational conditions and once they appear general relativity loses its predictive power. One proposal in order to eliminate those singularities was the quantization of general relativ-

ity. Unfortunately, it was shown that general relativity is not perturbatively renormalizable [3]. After that discovery many geometrical theories of gravity, different from general relativity and perturbatively renormalizable, have been introduced. Regrettably, those theories produce massive ghosts in their physical spectrum and they are not unitary theories[4].

In 2009 Petr Hořava introduced a geometrical theory of gravity with a different property [5]. In his theory, nowadays known as Hořava-Lifshitz theory (HL), there is an anisotropic scaling between space and time. His inspiration came from condensed matter physics where that anisotropy between space and time is common and it is represented by a dynamical critical exponent z [6, 7, 8, 9]. For physical systems which satisfy Lorentz invariance $z = 1$. The main motivation, of Hořava, for the introduction of that anisotropy is that it improves the short distance behavior of the theory. That anisotropy means that the Lorentz symmetry is broken, at least at high energies, where that asymmetry between space and time takes place. At low energies the HL theory tends to GR, recovering the Lorentz symmetry. As discussed by Hořava [5], a theory of gravity using those ideas is power-counting renormalizable, in 3+1 dimensions, for $z = 3$. Besides, GR is recovered when $z \rightarrow 1$. The HL theory was formulated, originally, with the aid of the Arnowitt-Deser-Misner (ADM) formalism [10]. In the ADM formalism the four dimensional metric $g_{\mu\nu}$ ($\mu, \nu = 0, 1, 2, 3$) is decomposed in terms of the three dimensional metric h_{ij} ($i, j = 1, 2, 3$), of spatial sections, the shift vector N_i and the lapse function \mathcal{N} , which is viewed as a gauge field for time reparametrizations. In general all those quantities depend both on space and time. In his original work, Hořava considered the simplified assumption that \mathcal{N} should depend only on time [5]. This assumption has become known as the *projectable condition*. Although many works have been written about HL theory using the *projectable condition*, some authors have considered the implications of working in the *non-projectable condition*. In other words, they have considered \mathcal{N} as a function of space and time [11, 12]. The gravitational action of the HL theory was proposed such that the kinetic component was constructed separately from the potential one. The kinetic component was motivated by the one coming from GR, written in terms of the extrinsic curvature tensor. It contains time derivatives of the spatial metric up to the second order and one free parameter (λ), which is not present in the general relativity kinetic component. At the limit when $\lambda \rightarrow 1$, one recovers GR kinetic component. The potential component must depend only on the spatial metric and its spatial derivatives. As a geometrical theory of gravity, the potential component

of the HL theory should be composed of scalar contractions of the Riemann tensor and its spatial derivatives.

In his original paper [5], Hořava considered a simplification in order to reduce the number of possible terms contributing to the potential component of his theory. It is called the *detailed balance condition*. Although this condition indeed reduces the number of terms contributing to the potential component, some authors have shown that, without using this condition, it is possible to construct a well defined and phenomenologically interesting theory, without many more extra terms [13, 14]. Like other geometrical theories of gravity, it was shown that the projectable version of the HL theory, with the detailed balance condition, have massive ghosts and instabilities [14, 15]. The HL theory have been applied to cosmology and produced very interesting models [16, 17, 18, 19, 20, 21, 22, 23]. For a recent review on some aspects of the HL theory see Ref.[24].

One of the first attempts to quantize the gravitational interaction was the canonical quantization of general relativity (CQGR). When applied to homogeneous cosmological spacetimes, the CQGR gives rise to quantum cosmology (QC). Although many physicists believe that QC is not the correct theory to describe the Universe, at the quantum level, an important point was raised by that theory. It is related to the interpretation of that quantum theory of the whole Universe. The *Copenhagen* interpretation of quantum mechanics cannot be applied to that theory because it is not possible to apply a statistical interpretation to a system composed of the entire Universe. One cannot repeat the experiments for that system. Two important interpretations of quantum mechanics that can be used in QC are: the *Many Worlds*[25] and the *DeBroglie-Bohm*[26, 27] interpretations. In many aspects they lead to the same results as the *Copenhagen* interpretation and can be applied to a system composed of the entire Universe. The *Many Worlds* is the interpretation most commonly used in QC, although the *DeBroglie-Bohm* interpretation has been applied to several models of quantum cosmology with great success [23, 28, 29, 30, 31, 32, 33, 34]. For more references on the use of the *DeBroglie-Bohm* interpretation in QC see Ref.[35]. In most of those models, the authors compute the scale factor trajectory and shows that this quantity never vanishes. That result gives a strong indication that those models are free from singularities, at the quantum level. Another important quantity introduced by the *DeBroglie-Bohm* interpretation is the quantum potential (Q) [26, 27]. For those quantum cosmology models, the determination of Q helps understanding why the scale factor never vanishes.

In the present paper, we canonically quantize an homogeneous and isotropic Hořava-Lifshitz cosmological model, with constant positive spatial sections and coupled to radiation. We consider the projectable version of that gravitational theory without the detailed balance condition. We use the ADM formalism to write the gravitational hamiltonian of the model and the Schutz variational formalism to write the perfect fluid hamiltonian. We find the Wheeler-DeWitt equation for the model. That equation depends on several parameters coming from the HL theory. We study the case where the values of the HL parameters are chosen, such that, the solutions to the Wheeler-DeWitt equation are bounded. Initially, we solve it using the *Many Worlds* interpretation. Using wavepackets computed with the solutions to the Wheeler-DeWitt equation, we obtain the scalar factor expected value $\langle a \rangle$. We show that this quantity oscillate between maxima and minima values and never go to zero. That result gives an indication that the model is free from singularities, at the quantum level. We improve this result by showing that if we subtract a standard deviation of a from $\langle a \rangle$, this quantity is still positive. We, also, study how the scale factor expected value depends on each of the HL parameter. Then, we use the *DeBroglie-Bohm* interpretation. We compute the Bohm's trajectories for the scale factor and show that it never goes to zero. We show that each trajectory agrees with the corresponding $\langle a \rangle$. We also compute the quantum potential. That quantity helps understanding why the scale factor never vanishes. It is important to mention that in Refs.[18, 23], the authors studied the QC version of the present model with $k \neq 0$, but neglecting the HL parameters g_C , g_Λ and g_r . They studied the models using the *Many Worlds* interpretation[18, 23] and the *DeBroglie-Bohm* interpretation[23]. In Ref.[17], the authors studied the QC version of the present model with $k = 1$, but neglecting the HL parameter g_Λ . They studied the models using the *Many Worlds* interpretation. Here, we will study the QC version of the present model with $k = 1$, without neglecting any HL parameter and using both *Many Worlds* and *DeBroglie-Bohm* interpretations. Taking in account the current cosmological observations, the present model will not be able to describe the present accelerated expansion of our Universe[36]. It is not our intention to describe the present stage of our Universe with the model introduced here. On the other hand, it is our intention to describe a 'possible' stage of our primordial Universe. Of course, after that initial stage the Universe would have to undergo a transition where the HL parameters would change to allow an accelerated expansion.

In Section 2, we construct the classical version of the homogeneous and

isotropic HL cosmological model, with constant positive spatial sections and coupled to radiation. In Section 3, we quantize the classical version of the model and solve the resulting Wheeler-DeWitt equation. Using the solutions, we construct wavepackets and compute the scale factor expected values. We study how the scale factor expected value depends on each of the HL parameter. Finally, we evaluate the behavior of the scale factor expected value after subtracting, from it, a standard deviation of a . In Section 4, we compute the Bohm's trajectories for the scale factor and the corresponding quantum potentials. We investigate how they depend on the HL parameters. We, also, compare the Bohm's trajectories for the scale factor with the corresponding expected values of that quantity. The Section 5 summarizes our main points and results.

2 Classical Hořava-Lifshitz model coupled to radiation

In the present work, we shall consider homogeneous and isotropic spacetimes. They are described by the Friedmann-Robertson-Walker (FRW) line element, given by,

$$ds^2 = -\mathcal{N}(t)^2 dt^2 + a(t)^2 \left(\frac{dr^2}{1 - kr^2} + r^2 d\Omega^2 \right), \quad (1)$$

where $d\Omega^2$ is the line element of the two-dimensional sphere with unitary radius, $a(t)$ is the scale factor, $\mathcal{N}(t)$ is the lapse function[37] and k represents the constant curvature of the spatial sections. The curvature is positive for $k = 1$, negative for $k = -1$ and zero for $k = 0$. Here, we are using the natural unit system, where $c = 8\pi G = \hbar = 1$. We assume that the matter content of the model is represented by a perfect fluid with four-velocity $U^\mu = \delta_0^\mu$ in the co-moving coordinate system used. The energy-momentum tensor is given by,

$$T_{\mu\nu} = (\rho + p)U_\mu U_\nu + pg_{\mu\nu}, \quad (2)$$

where ρ and p are the energy density and pressure of the fluid, respectively. The Greek indices μ and ν run from zero to three. The equation of state for a perfect fluid is $p = \omega\rho$, where ω is a constant that gives the type of fluid.

The action for the projectable HL gravity, without the detailed balance

condition, for $z = 3$ and in $3 + 1$ -dimensions is given by [16],

$$\begin{aligned} \mathcal{S}_{HL} = & \frac{M_p^2}{2} \int d^3x dt \mathcal{N} \sqrt{h} \left[K_{ij} K^{ij} - \lambda K^2 - g_0 M_p^2 - g_1 R - M_p^{-2} (g_2 R^2 + g_3 R_{ij} R^{ij}) \right. \\ & \left. - M_p^{-4} (g_4 R^3 + g_5 R R^i_j R^j_i + g_6 R^i_j R^j_k R^k_i + g_7 R \nabla^2 R + g_8 \nabla_i R_{jk} \nabla^i R^{jk}) \right], \end{aligned} \quad (3)$$

where g_i and λ are parameters associated with HL gravity, M_p is the Planck mass, K_{ij} are the components of the extrinsic curvature tensor and K represents its trace, R_{ij} are the components of the Ricci tensor computed for the metric of the spatial sections h_{ij} , R is the Ricci scalar computed for h_{ij} , h is the determinant of h_{ij} and ∇_i represents covariant derivatives. The Latin indices i and j run from one to three. As we have mentioned above, the GR kinetic component is recovered in the limit $\lambda \rightarrow 1$.

Introducing the metric of the spatial sections that comes from the FRW space-time (1), in the action (3) and using the following choices: $g_0 M_p^2 = 2\Lambda$ and $g_1 = -1$, we can write that,

$$\begin{aligned} \mathcal{S}_{HL} = & \kappa \int dt \mathcal{N} \left[-\frac{\dot{a}^2 a}{\mathcal{N}^2} + \frac{1}{3(3\lambda - 1)} \left(6ka - 2\Lambda a^3 - \frac{12k^2}{a M_p^2} (3g_2 + g_3) \right. \right. \\ & \left. \left. - \frac{24k^3}{a^3 M_p^4} (9g_4 + 3g_5 + g_6) \right) \right], \end{aligned} \quad (4)$$

where

$$\kappa = \frac{3(3\lambda - 1)M_p^2}{2} \int d^3x \frac{r^2 \sin\theta}{\sqrt{1 - kr^2}}.$$

If we choose, for simplicity, $\kappa = 1$, we will write the HL Lagrangian density (\mathcal{L}_{HL}), from \mathcal{S}_{HL} in Eq. (4) as,

$$\mathcal{L}_{HL} = \mathcal{N} \left[-\frac{\dot{a}^2 a}{\mathcal{N}^2} + g_c k a - g_\Lambda a^3 - g_r \frac{k^2}{a} - g_s \frac{k^3}{a^3} \right], \quad (5)$$

where the new parameters are defined by,

$$\begin{aligned} g_c &= \frac{2}{3\lambda - 1}, & g_\Lambda &= \frac{2\Lambda}{3(3\lambda - 1)}, & g_r &= \frac{4}{(3\lambda - 1)M_p^2} (3g_2 + g_3), \\ g_s &= \frac{8}{(3\lambda - 1)M_p^4} (9g_4 + 3g_5 + g_6). \end{aligned} \quad (6)$$

The parameter g_c is positive, by definition, and the others may be positive or negative.

Now, we want to write the HL Hamiltonian density. To accomplish the task, we must compute the momentum canonically conjugated to the single dynamical variable, present in the geometry sector, i.e., the scale factor. Using the definition, that momentum (P_a) is given by,

$$P_a = \frac{\partial \mathcal{L}}{\partial \dot{a}} = \frac{\partial}{\partial \dot{a}} \left[-\frac{\dot{a}^2 a}{\mathcal{N}} \right] = -\frac{2\dot{a}a}{\mathcal{N}} . \quad (7)$$

Introducing P_a (7) into the definition of the Hamiltonian density, with the aid of \mathcal{L}_{HL} (5), we obtain, the following HL Hamiltonian (H_{HL}),

$$H_{HL} = \mathcal{N} \mathcal{H}_{HL} = \mathcal{N} \left[-\frac{P_a^2}{4a} - g_c k a + g_\Lambda a^3 + g_r \frac{k^2}{a} + g_s \frac{k^3}{a^3} \right] . \quad (8)$$

In this work, we will obtain the perfect fluid Hamiltonian (H_{pf}) using the Schutz's variational formalism [38, 39]. In this formalism the four-velocity (U_ν) of the fluid is expressed in terms of six thermodynamical potentials (μ , ϵ , ζ , β , θ , S), in the following way,

$$U_\nu = \frac{1}{\mu} (\epsilon_{,\nu} + \zeta \beta_{,\nu} + \theta S_{,\nu}) , \quad (9)$$

where μ is the specific enthalpy, S is the specific entropy, ζ and β are connected to rotation and they are absent from the FRW models. Finally, ϵ and θ have no clear physical meaning. The four-velocity obeys the normalization condition,

$$U^\nu U_\nu = -1. \quad (10)$$

The starting point, in order to write the H_{pf} for the perfect fluid, is the action (\mathcal{S}_{pf}), which in this formalism is written as,

$$\mathcal{S}_{pf} = \int d^4x \sqrt{-g} (16\pi p) , \quad (11)$$

where g is the determinant of the four-dimensional metric ($g_{\alpha\beta}$) and p is the fluid pressure. Introducing the metric (1), Eqs. (9) and (10), the fluid equation of state and the first law of thermodynamics into the action (11), and after some thermodynamical considerations, the action takes the form [40],

$$\mathcal{S}_{pf} = \int dt \left[\mathcal{N}^{-1/\omega} a^3 \frac{\omega(\dot{\epsilon} + \theta \dot{S})^{1+1/\omega}}{(\omega + 1)^{1+1/\omega}} e^{-S/\omega} \right] . \quad (12)$$

From this action, we can obtain the perfect fluid Lagrangian density and write the Hamiltonian (H_{pf}),

$$H_{pf} = \mathcal{N}\mathcal{H}_{pf} = \mathcal{N} \left(P_\epsilon^{\omega+1} a^{-3\omega} e^S \right), \quad (13)$$

where

$$P_\epsilon = \mathcal{N}^{-1/\omega} a^3 (\dot{\epsilon} + \theta \dot{S})^{(\omega+1)^{-1/\omega}} e^{-S/\omega}.$$

We can further simplify the Hamiltonian (13), by performing the following canonical transformations [41],

$$T = -P_S e^{-S} P_\epsilon^{-(\omega+1)}, \quad P_T = P_\epsilon^{\omega+1} e^S, \quad \bar{\epsilon} = \epsilon - (\omega+1) \frac{P_S}{P_\epsilon}, \quad \bar{P}_\epsilon = P_\epsilon, \quad (14)$$

where $P_S = \theta P_\epsilon$. With these transformations the Hamiltonian (13) takes the form,

$$H_{pf} = \mathcal{N}\mathcal{H}_{pf} = \mathcal{N} \frac{P_T}{a^{3\omega}}, \quad (15)$$

where P_T is the momentum canonically conjugated to T . We can write now the total Hamiltonian of the model (H), which is written as the sum of H_{HL} (8) with H_{pf} (15),

$$H = \mathcal{N}\mathcal{H} = \mathcal{N} \left[-\frac{P_a^2}{4a} - g_c a + g_\Lambda a^3 + \frac{g_r}{a} + \frac{g_s}{a^3} + \frac{P_T}{a} \right]. \quad (16)$$

In H (16), we set $k = 1$, in order to consider, only, spacelike hypersurfaces with positive constant curvatures and $\omega = 1/3$, which restrict the matter content of the universe to be radiation. The classical dynamics is governed by the Hamilton's equations, derived from eq. (16).

In order to have an idea of the scale factor classical behavior, let us derive the Friedmann equation from H (16). The Friedmann equation is obtained by varying H , with respect to \mathcal{N} , and equating the resulting equation to zero. In the ADM formalism that equation is also known as the superhamiltonian constraint equation[37]. Now, in the conformal gauge $\mathcal{N} = a$, we have that: $P_a = -2\dot{a}$, where the dot means derivative with respect to the conformal time. Therefore, we may write the Friedmann equation in terms of \dot{a} , as,

$$\dot{a}^2 + V_c(a) = 0, \quad (17)$$

where,

$$V_c(a) = g_c a^2 - g_\Lambda a^4 - g_r - \frac{g_s}{a^2} - P_T. \quad (18)$$

The scale factor behavior depends on the shape of the classical potential $V_c(a)$ (18). On the other hand, the shape of $V_c(a)$ depends on the values of the parameters present in it. The parameters g_c and P_T are positive. The first is positive because it is associated to the curvature coupling constant and the second because it is related to the fluid energy density. The other parameters may be positive or negative. In the present work, we shall study the models where: g_r is positive and g_s and g_Λ are negative. For those choices, $V_c(a)$ (18) produces models where the scale factor is bounded. In other words, it oscillates between maxima and minima values. Those models are free from the big bang singularity.

3 Many Worlds Interpretation

3.1 Eigenvalue equation and the spectral method

We wish to quantize the model following the Dirac formalism for quantizing constrained systems [42]. First we introduce a wave-function which is a function of the canonical variables \hat{a} and \hat{T} ,

$$\Psi = \Psi(\hat{a}, \hat{T}). \quad (19)$$

Then, we impose the appropriate commutators between the operators \hat{a} and \hat{T} and their conjugate momenta \hat{P}_a and \hat{P}_T . Working in the Schrödinger picture, the operators \hat{a} and \hat{T} are simply multiplication operators, while their conjugate momenta are represented by the differential operators

$$\hat{P}_a \rightarrow -i \frac{\partial}{\partial a}, \quad \hat{P}_T \rightarrow -i \frac{\partial}{\partial T}. \quad (20)$$

Finally, we demand that the operator corresponding to H (16) (\hat{H}) annihilate the wave-function Ψ , which leads to Wheeler-DeWitt equation,

$$\left(-\frac{1}{4} \frac{\partial^2}{\partial a^2} + g_c a^2 - g_\Lambda a^4 - g_r - \frac{g_s}{a^2} \right) \psi(a, \tau) = i \frac{\partial}{\partial \tau} \psi(a, \tau). \quad (21)$$

where the new variable $\tau = -T$ has been introduced.

The operator \hat{H} is self-adjoint [43] with respect to the internal product,

$$(\Psi, \Phi) = \int_0^\infty da \Psi(a, \tau)^* \Phi(a, \tau), \quad (22)$$

if the wave functions are restricted to the set of those satisfying either $\Psi(0, \tau) = 0$ or $\Psi'(0, \tau) = 0$, where the prime \prime means the partial derivative with respect to a . Here, we consider wave functions satisfying the former type of boundary condition and we also demand that they vanish when a goes to ∞ .

The Wheeler-DeWitt equation (21) may be solved by writing $\Psi(a, \tau)$ as,

$$\Psi(a, \tau) = e^{-iE\tau} \eta(a) \quad (23)$$

in which $\eta(a)$ depends solely on a and satisfies the eigenvalue equation

$$-\frac{d^2\eta(a)}{da^2} + V(a)\eta(a) = 4E\eta(a), \quad (24)$$

in which the potential $V(a)$ is

$$V(a) = 4g_c a^2 - 4g_\Lambda a^4 - 4g_r - \frac{4g_s}{a^2}. \quad (25)$$

In the same way as in the classical regime, the potential $V(a)$ gives rise to bound states. Therefore, the possible values of the energy E in Eq.(24) of those states will belong to a discrete set of eigenvalues E_n , in which $n \in \{1, 2, 3, \dots\}$. For each eigenvalue E_n , there will be a corresponding eigenvector $\eta_n(a)$. The general solution to the Wheeler-DeWitt equation (21) is a linear combination of all those eigenvectors,

$$\Psi(a, \tau) = \sum_{n=1}^{\infty} C_n \eta_n(a) e^{-iE_n \tau}, \quad (26)$$

where C_n are constant coefficients to be specified.

We will use the Galerkin or spectral method (SM)[44], in order to solve the eigenvalue equation (24). This method has already been used in quantum cosmology[45, 46, 47] and also in several areas of classical general relativity[48, 49, 50, 51]. One important condition of the SM is that the functions, which are solutions to the equation we want to solve, must fall sufficiently fast for large values of the variable. In the present situation that variable is the scale factor a . Taking in account that property of the solution, we restrict the domain of a to: $0 < a < L$, in which L is a real number to be suitably chosen. As we have mentioned above, we shall consider, here, wavefunctions satisfying the condition $\Psi(0, \tau) = 0$. It is convenient, then, to choose our

basis functions to be sine functions. Therefore, we may write $\eta_n(a)$ in Eq. (24) as,

$$\eta(a) \approx \sum_{n=1}^N A_n \sqrt{\frac{2}{L}} \sin\left(\frac{n\pi a}{L}\right), \quad (27)$$

in which the coefficients A_n are yet to be determined, and a finite number N of base functions has been chosen. For the same domain of a , we also use the same basis to expand the terms of Eq. (24),

$$V(a)\eta(a) \approx \sum_{n=1}^N \sum_{m=1}^N C_{m,n} A_m \sqrt{\frac{2}{L}} \sin\left(\frac{n\pi a}{L}\right), \quad (28)$$

$$4\eta(a) \approx \sum_{n=1}^N \sum_{m=1}^N C'_{m,n} A_m \sqrt{\frac{2}{L}} \sin\left(\frac{n\pi a}{L}\right), \quad (29)$$

in which $V(a)$ is given in Eq. (25) and the coefficients $C_{m,n}$ and $C'_{m,n}$ can be easily determined to be,

$$C_{m,n} = \frac{2}{L} \int_0^L \sin\left(\frac{m\pi a}{L}\right) V(a) \sin\left(\frac{n\pi a}{L}\right) da, \quad (30)$$

$$C'_{m,n} = \frac{2}{L} \int_0^L \sin\left(\frac{m\pi a}{L}\right) 4 \sin\left(\frac{n\pi a}{L}\right) da. \quad (31)$$

Introducing the results Eqs. (27)-(31) into the eigenvalue equation (24) and due to orthonormality of the basis functions, we obtain,

$$\left(\frac{n\pi}{L}\right)^2 A_n + \sum_{m=1}^N C_{m,n} A_m = E \sum_{m=1}^N C'_{m,n} A_m. \quad (32)$$

The last equation (32), may be written in a compact notation as,

$$C'^{-1} D A = E A, \quad (33)$$

where C' is the $N \times N$ square matrix the elements of which are given by (31) and D is a $N \times N$ square matrix with elements of the form,

$$D_{m,n} = \left(\frac{n\pi}{L}\right)^2 \delta_{m,n} + C_{m,n}. \quad (34)$$

The solution to Eq. (33) gives the eigenvalues and corresponding eigenfunctions to the bound states of our quantum cosmology model.

3.2 Scale factor expected values and standard deviations

In the present subsection we solve the eigenvalue equation (24), using the SM. In order to understand how each HL parameter modifies the scale factor expected value ($\langle a \rangle$), we compute $\langle a \rangle$ fixing all parameters but one. That calculation, enable us to learn how $\langle a \rangle$ depends on the HL parameter which varied. Then, we repeat the calculation, in the same manner, for all HL parameters. We also study how $\langle a \rangle$ depends on the number of base functions N , present in $\eta_n(a)$ (27). We consider the cases where $2 \leq N \leq 10$. An important ingredient in the SM is L . In order to improve our results, we compute the best value of L for each value of a given HL parameter.

We compute the scale factor expected value, using the following expression,

$$\langle a \rangle = \frac{\int_0^\infty a |\Psi(a, \tau)|^2 da}{\int_0^\infty |\Psi(a, \tau)|^2 da}, \quad (35)$$

where $\Psi(a, \tau)$ is given by Eq. (26). In order to compute $\Psi(a, \tau)$, we use the eigenvectors $\eta_n(a)$ and eigenvalues E_n , derived from Eq. (24) with the SM. We, also, set all coefficients C_n equal to one in Eq. (26).

As we shall see, for all HL parameters and N values considered, $\langle a \rangle$ oscillates between maxima and minima values and never vanishes. It gives an initial indication that those models are free from singularities, at the quantum level. The domain where $\langle a \rangle$ oscillates depends on the mean energy (\bar{E}) of the wavepacket considered. That quantity is specified by the number N , of base functions contributing to the wavepacket, and the energy eigenvalues of those N base functions. We may improve the result that $\langle a \rangle$ never vanishes by computing $\langle a \rangle - \sigma_a$, where σ_a stands for the standard deviation of a . If this quantity is always positive like $\langle a \rangle$, it will be a stronger indication that the model is free from singularities, at the quantum level. We compute $\langle a \rangle - \sigma_a$, for the present model. By definition the standard deviation of a is given by,

$$\sigma_a = \sqrt{\langle a^2 \rangle - \langle a \rangle^2}, \quad (36)$$

where,

$$\langle a^2 \rangle = \frac{\int_0^\infty a^2 |\Psi(a, \tau)|^2 da}{\int_0^\infty |\Psi(a, \tau)|^2 da}, \quad (37)$$

and $\langle a \rangle^2$ is given by the square of Eq. (35). Using the wavefunction (26) and repeating some procedures we did in order to compute $\langle a \rangle$, we computed

$\langle a \rangle - \sigma_a$ for all HL parameters and N values, considered. Let us, now, present our results on how $\langle a \rangle$, depends on the HL parameters (g_c, g_r, g_s, g_Λ) and N . The values of the HL parameters and N , in the figures below, were chosen for a better visualization of the results.

3.2.1 Results for g_c

If we fix N , along with the other HL parameters, and vary g_c we observe the following properties of $\langle a \rangle$: (i) the maximum value of $\langle a \rangle$ decreases with the increase of g_c ; (ii) the amplitude of oscillation for $\langle a \rangle$ decreases with the increase of g_c ; (iii) the number of $\langle a \rangle$ oscillations, for a fixed τ interval, increases with the increase of g_c . Those behaviors may be understood by observing the potential, that confines the scale factor. When one increases g_c , $\langle a \rangle$ is forced to oscillate in an ever decreasing region. Under those conditions, for fixed N and the other HL parameters, the maximum value and the amplitude of $\langle a \rangle$ decrease. Also, since the domain where $\langle a \rangle$ oscillates is decreasing, the number of $\langle a \rangle$ oscillations, for a fixed τ interval, increases. All those properties can be seen in Figures 1 and 2. Each figure shows examples of the behavior of $V(a)$ and $\langle a \rangle$, for two different values of g_c while the τ interval, N and the other HL parameters remain fixed.

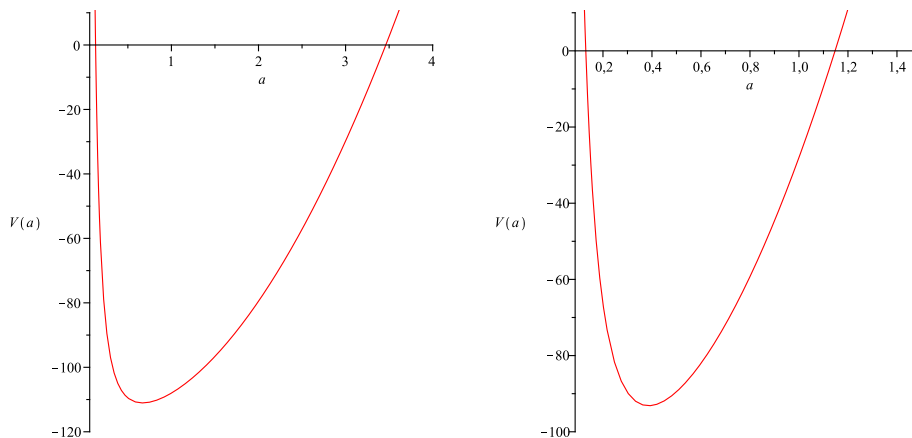


Figure 1: The figures show the potential $V(a)$ for $g_s = -2$, $g_r = 120$, $g_\Lambda = 0$. In the left $V(a)$ we used $g_c = 10$ and in the right one $g_c = 90$.

For $g_c = 10$, we have that $\bar{E} = -104.592479205836$. Therefore, from $V(a)$ Figure 1, the domain where $\langle a \rangle$ oscillates is: $[0.3782813789, 1.182224715]$,

which has the length: 0.8039433361. On the other hand, for $g_c = 90$, we have that $\bar{E} = -73.7774376335110$. Therefore, the domain where $\langle a \rangle$ oscillates is: $[0.2184008560, 0.6825577576]$, which has the length: 0.4641569016.

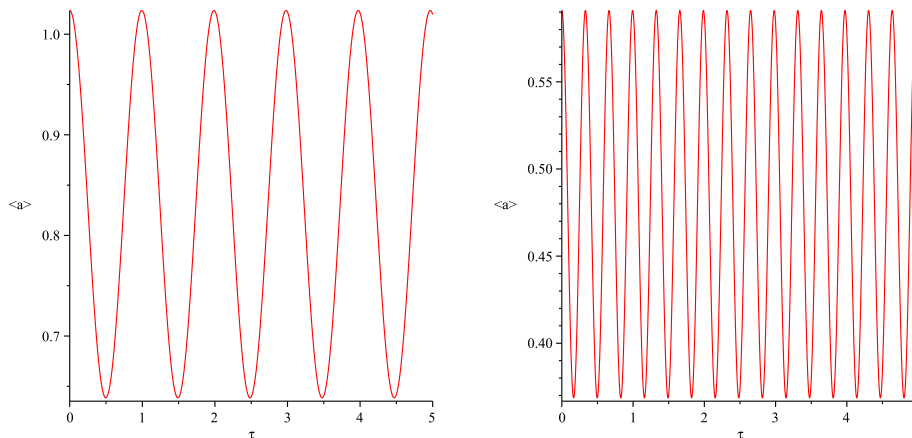


Figure 2: The figures show the $\langle a \rangle$ for $N = 2$, $g_s = -2$, $g_r = 120$, $g_\Lambda = 0$. In the left $\langle a \rangle$ we used $g_c = 10$ and in the right one $g_c = 90$.

3.2.2 Results for g_Λ

If we fix N , along with the other HL parameters, and vary g_Λ we observe the following properties of $\langle a \rangle$: (i) the maximum value of $\langle a \rangle$ decreases with the decrease of g_Λ ; (ii) the amplitude of oscillation for $\langle a \rangle$ decreases with the decrease of g_Λ ; (iii) the number of $\langle a \rangle$ oscillations, for a fixed τ interval, increases with the decrease of g_Λ . Those behaviors may be understood by observing the potential, that confines the scale factor. When one decreases g_Λ , $\langle a \rangle$ is forced to oscillate in an ever decreasing region. Under those conditions, for fixed N and the other HL parameters, the maximum value and the amplitude of $\langle a \rangle$ decrease. Also, since the domain where $\langle a \rangle$ oscillates is decreasing, the number of $\langle a \rangle$ oscillations, for a fixed τ interval, increases. All those properties can be seen in Figures 3 and 4. Each figure shows examples of the behavior of $V(a)$ and $\langle a \rangle$, for two different values of g_Λ while the τ interval, N and the other HL parameters remain fixed.

For $g_\Lambda = -1$, we have that $\bar{E} = -103.833980119716$. Therefore, from $V(a)$ Figure 3, the domain where $\langle a \rangle$ oscillates is: $[0.3676565615, 1.137772203]$, which has the length: 0.7701156415. On the other hand, for $g_\Lambda = -25$, we

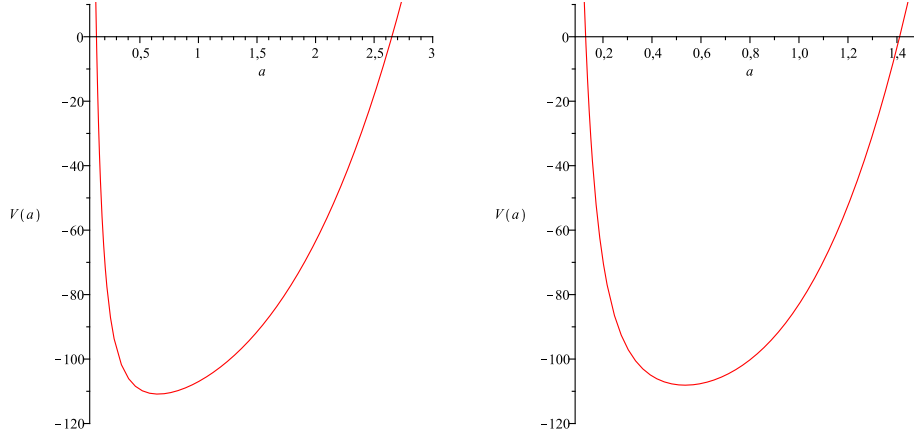


Figure 3: The figures show the potential $V(a)$ for $g_s = -2$, $g_r = 120$, $g_c = 10$. In the left $V(a)$ we used $g_\Lambda = -1$ and in the right one $g_\Lambda = -25$.

have that $\bar{E} = -95.6220677191430$. Therefore, the domain where $\langle a \rangle$ oscillates is: $[0.2927449802, 0.8679732690]$, which has the length: 0.5752282888 .

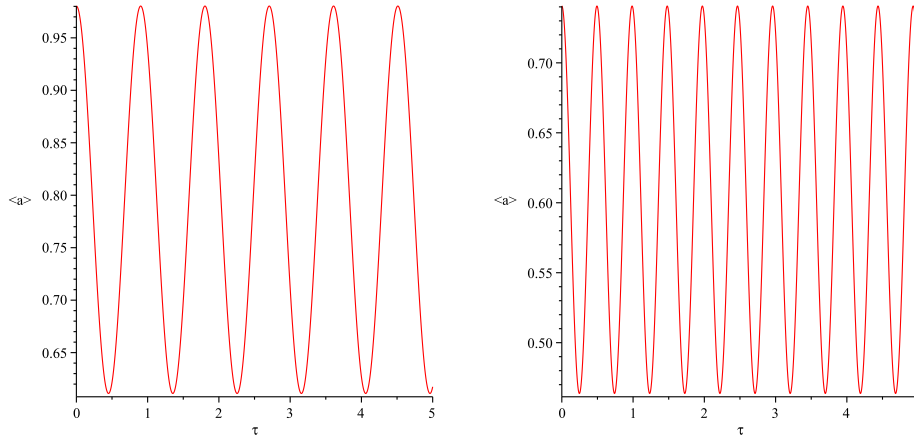


Figure 4: The figures show the $\langle a \rangle$ for $N = 2$, $g_s = -2$, $g_r = 120$, $g_c = 10$. In the left $\langle a \rangle$ we used $g_\Lambda = -1$ and in the right one $g_\Lambda = -25$.

3.2.3 Results for g_r

If we fix N , along with the other HL parameters, and vary g_r we observe the following properties of $\langle a \rangle$: its maximum value, its amplitude of oscillation and the number of $\langle a \rangle$ oscillations, for a fixed τ interval, do not vary with g_r . When one changes g_r , the size and the position of the interval where $\langle a \rangle$, is forced to oscillate, is not modified. Under those conditions, for fixed N and the other HL parameters, the maximum value of $\langle a \rangle$, the number of $\langle a \rangle$ oscillations and its amplitude are not modified, when one changes g_s . All those properties can be seen in Figure 5 and 6. It shows examples of the behavior of $\langle a \rangle$, for two different values of g_r while the τ interval, N and the other HL parameters remain fixed.

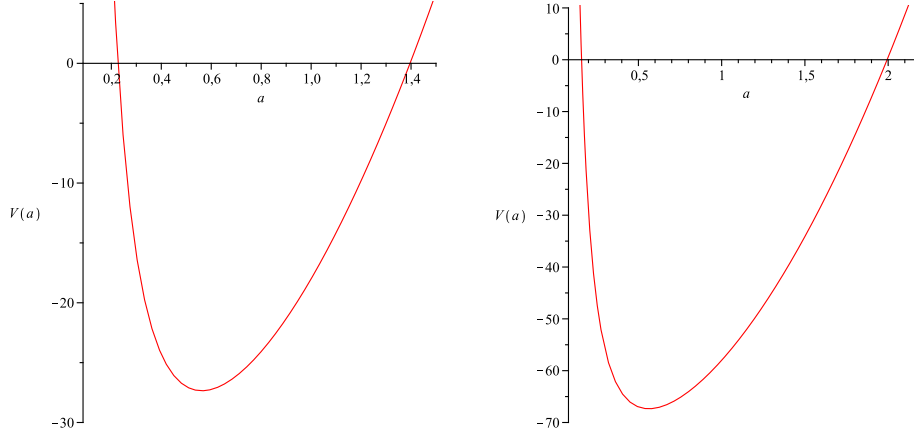


Figure 5: The figures show the potential $V(a)$ for $g_s = -2$, $g_\Lambda = 0$, $g_c = 20$. In the left $V(a)$ we used $g_r = 40$ and in the right one $g_r = 80$.

For $g_r = 40$, we have that $\bar{E} = -18.2104751421654$. Therefore, from $V(a)$ Figure 5, the domain where $\langle a \rangle$ oscillates is: $[0.3180954556, 0.9941285249]$, which has the length: 0.6760330693. On the other hand, for $g_r = 80$, we have that $\bar{E} = -58.2104751421655$. Therefore, the domain where $\langle a \rangle$ oscillates is: $[0.3180954556, 0.9941285249]$, which has the length: 0.6760330693.

3.2.4 Results for g_s

If we fix N , along with the other HL parameters, and vary g_s we observe the following properties of $\langle a \rangle$: (i) its amplitude of oscillation and the number

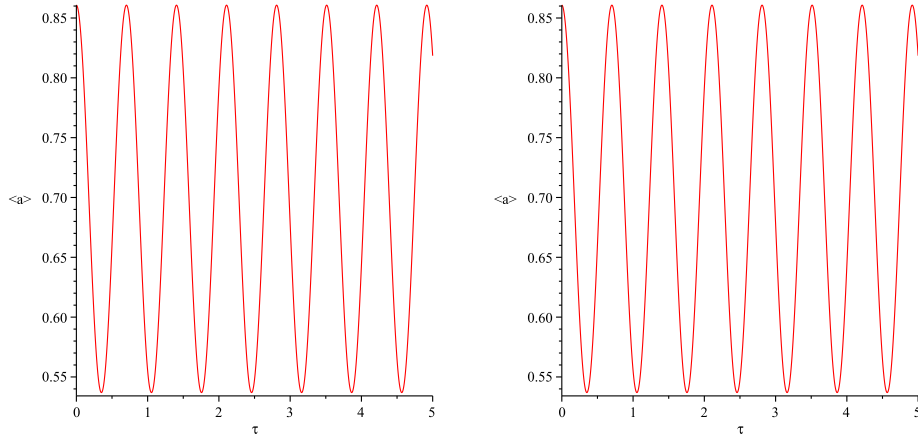


Figure 6: The figures show the $\langle a \rangle$ for $N = 2$, $g_s = -2$, $g_\Lambda = 0$, $g_c = 20$. In the left $\langle a \rangle$ we used $g_r = 40$ and in the right one $g_r = 80$.

of $\langle a \rangle$ oscillations, for a fixed τ interval, do not vary with g_s ; (ii) the maximum value of $\langle a \rangle$ increases with the decrease of g_s . Those behaviors may be understood by observing the potential, that confines the scale factor. When one decreases g_s , the size of the interval where $\langle a \rangle$, is forced to oscillate, is not modified. Under those conditions, for fixed N and the other HL parameters, the number of $\langle a \rangle$ oscillations and its amplitude are not modified, when one changes g_s . On the other hand, when one decreases g_s , all the interval where $\langle a \rangle$, is forced to oscillate, is shifted to the right, where the scale factor takes greater values. Under those conditions, for fixed N and the other HL parameters, the maximum value of $\langle a \rangle$ increases, when one decreases g_s . All those properties can be seen in Figures 7 and 8. Each figure shows examples of the behavior of $V(a)$ and $\langle a \rangle$, for two different values of g_s while the τ interval, N and the other HL parameters remain fixed.

For $g_s = -20$, we have that $\bar{E} = -70.9932768412420$. Therefore, from $V(a)$ Figure 7, the domain where $\langle a \rangle$ oscillates is: $[0.7192555414, 1.390326445]$, which has the length: 0.6710709036. On the other hand, for $g_s = -120$, we have that $\bar{E} = -13.0506261790150$. Therefore, the domain where $\langle a \rangle$ oscillates is: $[1.265657001, 1.935350368]$, which has the length: 0.669693367.

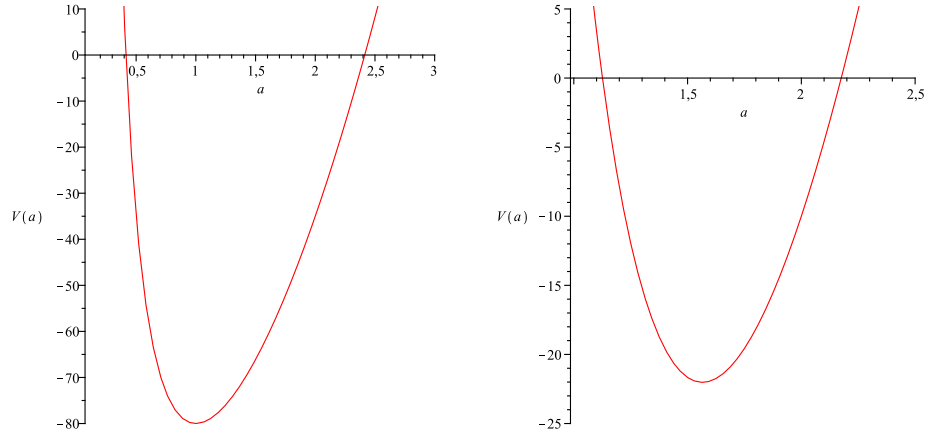


Figure 7: The figures show the potential $V(a)$ for $g_\Lambda = 0$, $g_r = 120$, $g_c = 20$. In the left $V(a)$ we used $g_s = -20$ and in the right one $g_s = -120$.

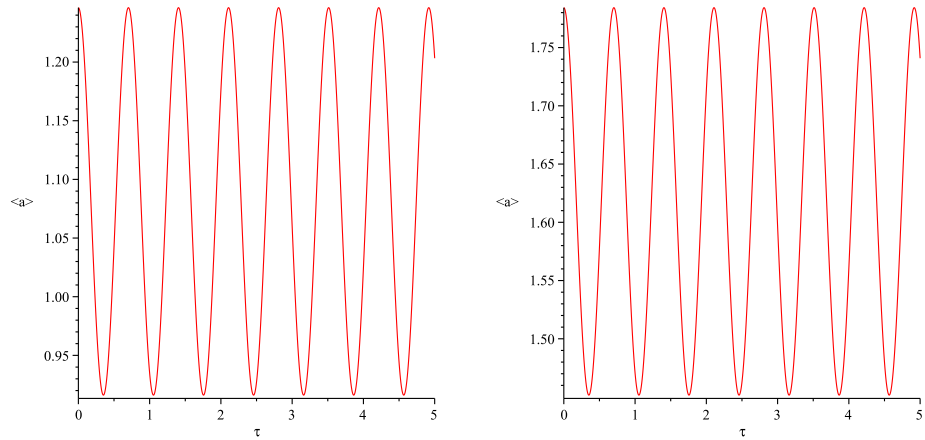


Figure 8: The figures show the $\langle a \rangle$ for $N = 2$, $g_\Lambda = 0$, $g_r = 120$, $g_c = 20$. In the left $\langle a \rangle$ we used $g_s = -20$ and in the right one $g_s = -120$.

3.2.5 Results for N

If we fix all the HL parameters and vary N we observe the following properties of $\langle a \rangle$: (i) the maximum value of $\langle a \rangle$ grows with the increase of N ; (ii) the amplitude of oscillation for $\langle a \rangle$ increases with the increase of N ; (iii) the number of $\langle a \rangle$ oscillations, for a fixed τ interval, remains constant with the increase of N . In order to understand those behaviors we notice that the

mean energy associated with the wavepacket increases with the increase of N . Therefore, for fixed values of the HL parameters, when we increase N the domain where $\langle a \rangle$ oscillates increases. In this way, the maximum value and the amplitude of $\langle a \rangle$ increase. On the other hand, the result that the number of $\langle a \rangle$ oscillations, for a fixed τ interval, remains constant, may be explained by the fact that the mean energy increases, when one increases N , and the potential energy is not modified. Therefore, in that case, the kinetic energy increases. That means that, $\langle a \rangle$ will oscillate more rapidly in a larger region. The most interesting result is that the oscillation velocity increases in such way that the oscillation frequency remains constant, when one increases N . All those properties can be seen in Figure 1, which gives an example for the potential $V(a)$, and Figures 2 and 9, which gives three examples of $\langle a \rangle$, for the same values of the HL parameters, with different values of N .

For $g_c = 10$, with $N = 5$, we have that $\bar{E} = -95.1047199335060$. Therefore, from $V(a)$ Figure 1, the domain where $\langle a \rangle$ oscillates is: $[1.551262998, 0.2882899909]$, which has the length: 1.262973007. On the other hand, for $g_c = 10$, with $N = 10$, we have that $\bar{E} = -79.2852819937343$. Therefore, the domain where $\langle a \rangle$ oscillates is: $[2.005428161, 0.2230015536]$, which has the length: 1.782426607. Those results must be compared with the results of the examples given in Figures 1 and 2, where $g_c = 10$ and $N = 2$.

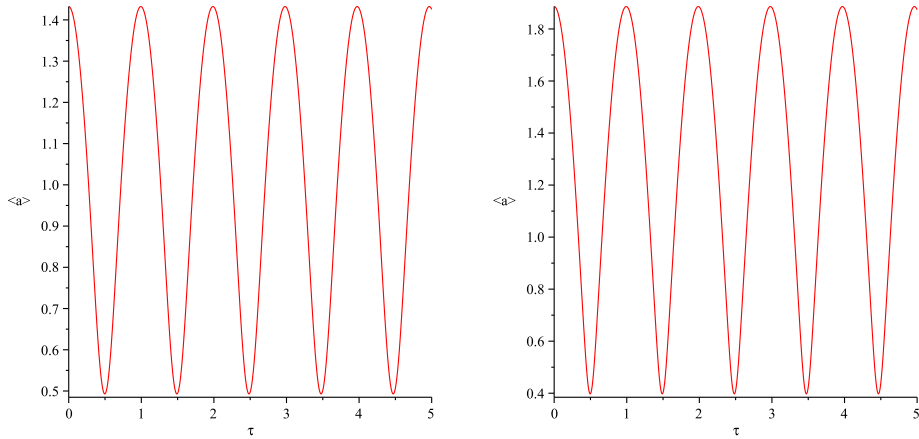


Figure 9: The figures show the $\langle a \rangle$ for $g_c = 10$, $g_\Lambda = 0$, $g_r = 120$, $g_s = -2$. In the left $\langle a \rangle$ we used $N = 5$ and in the right one $N = 10$.

3.2.6 Results for the standard deviations

We computed $\langle a \rangle - \sigma_a$, where $\langle a \rangle$ is given by eq. (35) and σ_a by eq. (36), for different domains of the HL parameters (g_c, g_r, g_s, g_Λ) and N values. For all computed cases, that quantity is always positive. That result gives a stronger indication that the present models are free from singularities, at the quantum level. As for the mathematical significance of that result, we may mention that if our distribution were a normal one and if one takes the interval $\langle a \rangle \pm \sigma_a$, around the mean value, it would cover over half the area under the distribution. More precisely, 68,26% [52]. Two examples of $\langle a \rangle$ and $\langle a \rangle - \sigma_a$, as a function of time, are shown in Figure 10.

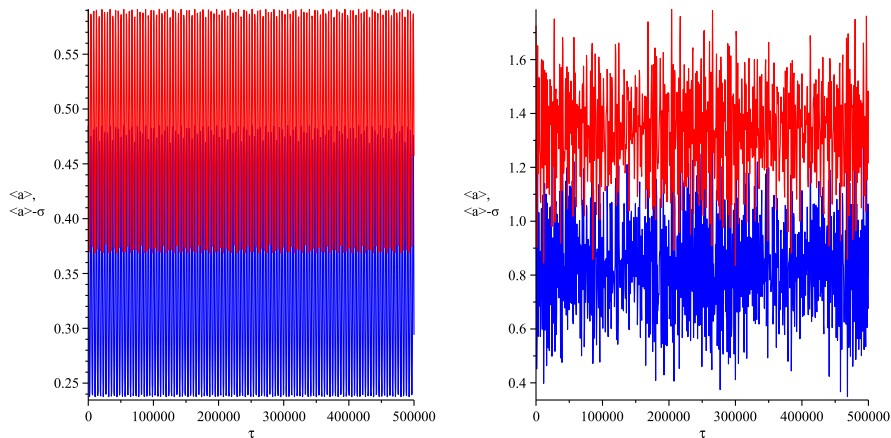


Figure 10: $\langle a \rangle$ and $\langle a \rangle - \alpha\sigma_a$ for two different models during the time interval $0 < \tau < 500000$. The left figure is for model with: $g_c = 90, g_r = 120, g_\Lambda = 0, g_s = -2$ and $N = 2$. The right figure is for model with: $g_s = -20, g_r = 120, g_\Lambda = 0, g_c = 20$ and $N = 10$.

4 DeBroglie-Bohm Interpretation

In this section, we want to apply the *DeBroglie-Bohm* interpretation of quantum mechanics[26, 27], to the present HL quantum cosmology model. Our main motivation is to compare the results we shall obtain with that interpretation with the ones we obtained in the previous section, where we used the *Many Worlds* interpretation of quantum mechanics. The *DeBroglie-Bohm* interpretation of quantum mechanics and related ideas have been used by many

authors in quantum cosmology over the years [23, 28, 29, 30, 31, 32, 33, 34]. In order to use the *DeBroglie-Bohm* interpretation we must re-write the quantum cosmology wavefunction $\Psi(a, \tau)$, in its polar form [27],

$$\Psi(a, \tau) = R(a, \tau)e^{iS(a, \tau)}, \quad (38)$$

where $R(a, \tau)$ is the wavefunction amplitude and $S(a, \tau)$ is its phase. Following the *DeBroglie-Bohm* interpretation we introduce $\Psi(a, \tau)$ Eq. (38) in Eq. (21), this leads to the next two equations for $R(a, \tau)$ and $S(a, \tau)$ [27],

$$\left(\frac{\partial S(a, \tau)}{\partial a}\right)^2 + Q(a, \tau) + 4\left(g_c k a^2 - g_\Lambda a^4 - g_r k^2 - \frac{g_s k}{a^2}\right) = 0, \quad (39)$$

$$2\frac{\partial R(a, \tau)}{\partial a}\frac{\partial S(a, \tau)}{\partial a} + R(a, \tau)\frac{\partial^2 S(a, \tau)}{\partial a^2} + \frac{4}{a^{3\omega-1}}\left(\frac{\partial R(a, \tau)}{\partial \tau}\right) = 0. \quad (40)$$

Where the Bohmian quantum potential $Q(a, \tau)$, in Eq. (39), is defined by [27],

$$Q(a, \tau) = -\frac{1}{R(a, \tau)}\frac{\partial^2 R(a, \tau)}{\partial a^2}. \quad (41)$$

The Bohmian trajectory of a is given by [27],

$$\frac{da(\tau)}{d\tau} = \frac{1}{mass}\frac{\partial S}{\partial a}, \quad (42)$$

where, from Eq. (16), the *mass*, for the present situation, is given by 2.

The solution to Eq. (42), which is the Bohmian trajectory of $a(\tau)$, which is the variable describing the universe, represents the quantum behavior for the cosmic evolution in the Planck era.

4.1 Bohmian trajectories of a

Using the wavepacket determined in the previous section Eq. (26), we obtain its polar form Eq. (38). Introducing the phase $S(a, \tau)$, in equation (42), we compute the Bohmian trajectories of a , for different values of all HL parameters. We use, here, the same procedure of the previous section, in order to investigate how the Bohmian trajectories of a depend on the HL parameters. We fix all parameters but one, and let that parameter vary over

a wide range of values. Then, we repeat the calculation, in the same manner, for all HL parameters. After solving Eq. (42), for many different values of g_c , g_Λ , g_r , g_s and N , we found the same qualitative behavior for the Bohmian trajectories of $a(\tau)$, in all those cases. They oscillate between maxima and minima values and never go through the zero value. It means that, quantum mechanically, in those models there are no singularities, which confirms the result obtained in the previous section using the *Many Worlds* interpretation. From our study, we also noticed that the Bohmian trajectories of a are, qualitatively, very similar to the corresponding expected values of a . That result, helps verifying the equivalence between both quantum mechanical interpretations. Next, let us compare some Bohmian trajectories of a , with the corresponding expected values of a . In order to better compare those two quantum mechanical interpretations, we used as initial conditions for $a(\tau)$ at $\tau = 0$, in the Bohmian trajectories of a , the expected values of a at $\tau = 0$, for the corresponding models.

4.1.1 Results for g_c

After solving equation (42), for several different values of g_c , N and various τ intervals, while leaving fixed the other HL parameters, we observe the following properties of a , from the Bohmian trajectories of a : (i) the maximum value of a decreases with the increase of g_c ; (ii) the amplitude of oscillation for a decreases with the increase of g_c ; (iii) the number of a oscillations, for a fixed τ interval, increases with the increase of g_c . Those behaviors are in agreement with those obtained, in the previous section, for the expected value of a . Two examples of those agreements, between $\langle a \rangle$ and the Bohmian trajectories of a , may be seen in Figures 2 and 11.

4.1.2 Results for g_Λ

After solving equation (42), for several different values of g_Λ , N and various τ intervals, while leaving fixed the other HL parameters, we observe the following properties of a , from the Bohmian trajectories of a : (i) the maximum value of a decreases with the decrease of g_Λ ; (ii) the amplitude of oscillation for a decreases with the decrease of g_Λ ; (iii) the number of a oscillations, for a fixed τ interval, increases with the decrease of g_Λ . Those behaviors are in agreement with those obtained, in the previous section, for the expected value of a . Two examples of those agreements, between $\langle a \rangle$ and the Bohmian

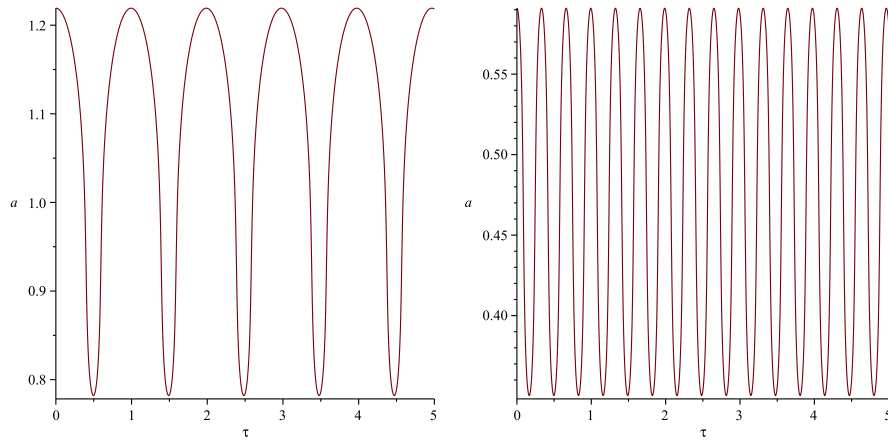


Figure 11: The figures show Bohmian trajectories of a for $N = 2$, $g_s = -2$, $g_r = 120$, $g_\Lambda = 0$. In the left Bohmian trajectory of a we used $g_c = 10$ and in the right one $g_c = 90$.

trajectories of a , may be seen in Figures 4 and 12.

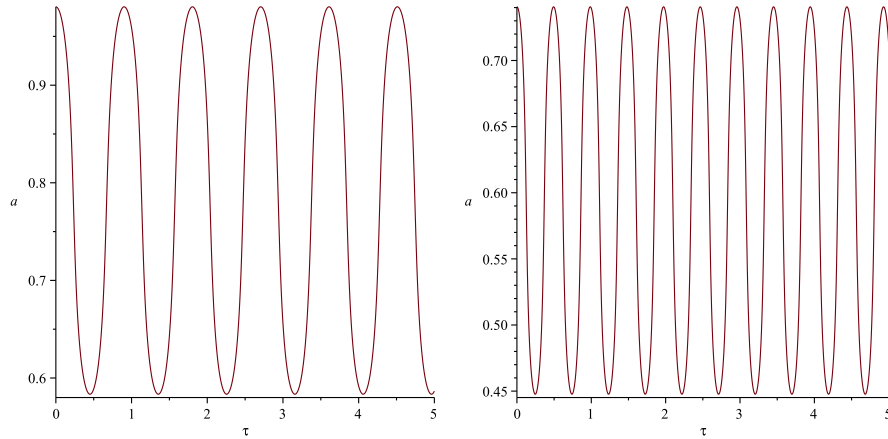


Figure 12: The figures show Bohmian trajectories of a for $N = 2$, $g_s = -2$, $g_r = 120$, $g_c = 10$. In the left Bohmian trajectory of a we used $g_\Lambda = -1$ and in the right one $g_\Lambda = -25$.

4.1.3 Results for g_r

After solving equation (42), for several different values of g_r , N and various τ intervals, while leaving fixed the other HL parameters, we observe the following properties of a , from the Bohmian trajectories of a : its maximum value, its amplitude of oscillation and the number of a oscillations, for a fixed τ interval, do not vary with g_r . Those behaviors are in agreement with those obtained, in the previous section, for the expected value of a . Two examples of those agreements, between $\langle a \rangle$ and the Bohmian trajectories of a , may be seen in Figures 6 and 13.

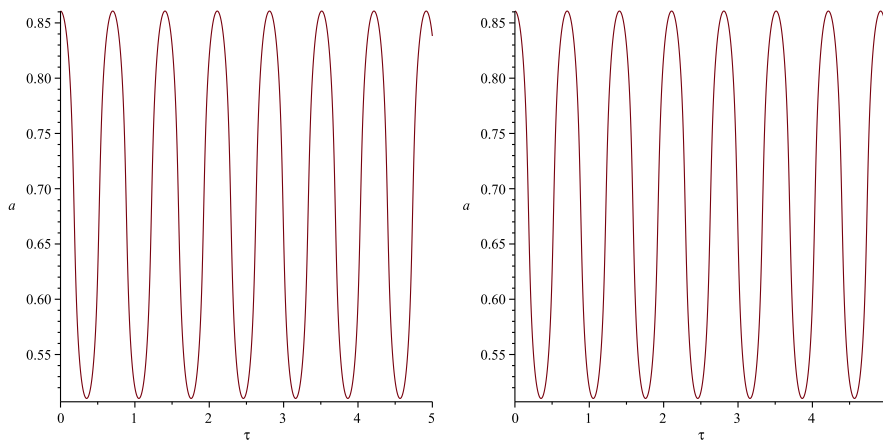


Figure 13: The figures show Bohmian trajectories of a for $N = 2$, $g_s = -2$, $g_\Lambda = 0$, $g_c = 20$. In the left Bohmian trajectory of a we used $g_r = 40$ and in the right one $g_r = 80$.

4.1.4 Results for g_s

After solving equation (42), for several different values of g_s , N and various τ intervals, while leaving fixed the other HL parameters, we observe the following properties of a , from the Bohmian trajectories of a : (i) its amplitude of oscillation and the number of a oscillations, for a fixed τ interval, do not vary with g_s ; (ii) the maximum value of a increases with the decrease of g_s . Those behaviors are in agreement with those obtained, in the previous section, for the expected value of a . Two examples of those agreements, between $\langle a \rangle$ and the Bohmian trajectories of a , may be seen in Figures 8 and 14.

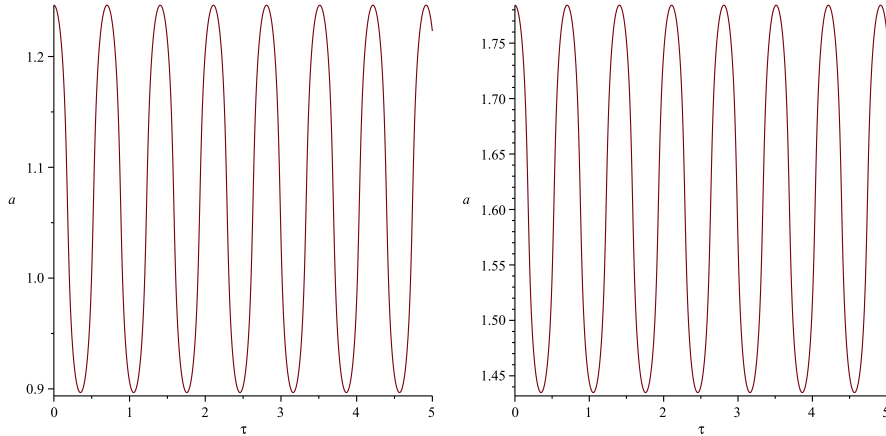


Figure 14: The figures show Bohmian trajectories of a for $N = 2$, $g_r = 120$, $g_\Lambda = 0$, $g_c = 20$. In the left Bohmian trajectory of a we used $g_s = -20$ and in the right one $g_s = -120$.

4.2 Bohmian quantum potential Q

The absence of singularities in the present models are very easy to understand when one observes the Bohmian quantum potential Eq. (41), for those models. We computed $Q(a, \tau)$ Eq. (41), for several values of the HL parameters and N . The calculations were made over the Bohmian trajectories of a . We obtained Q as a function of τ as well as a function of a . We found the same qualitative behavior of Q , in all those cases. Initially, considering Q as a function of τ , at $\tau = 0$, there is a potential barrier (B_0) that prevents the value of a to grow more than its maximum allowed value. Then, the barrier becomes a well for a brief moment and again a new barrier appears (B_1). B_1 prevents the value of a ever to go through zero. After a while, B_1 turns into a well for a brief moment and then another barrier identical to B_0 appears. After that, Q , periodically, repeats itself. B_0 is different from B_1 . B_0 exists for a longer period and is shorter than B_1 . One may interpret the potential shape in the following way. Initially, at $\tau = 0$, a is at its maximum value. It starts to decrease, first slowly, and then its velocity starts to increase until a reaches its minimum value different from zero. After that, a grows from its minimum value different from zero, first rapidly, and then its velocity starts to decrease until it goes to zero, at the maximum value of a . There, its velocity changes sign and a starts to decrease once more, as described above.

This dynamics is represented in Q , initially, by B_0 , then the first well, then B_1 and finally the well just after B_1 . Then, the movement of a repeats itself periodically. These models have no singularities because B_1 and its periodic repetitions prevent a ever to go through zero. In order to exemplify this behavior, we show, in Figure 15, the Bohmian quantum potential Eq. (41), for the model with $g_\Lambda = -1$, $g_c = 10$, $g_r = 120$, $g_s = -2$ and $N = 2$. In the left side of that figure, we show Q as a function of the time τ . For a better visualization of Q 's behavior, we choose a small time interval in Figure 15. In the right side of Figure 15, we show Q as a function of a . In this case, we may see clearly B_0 and B_1 . For a clearer understand of Q 's behavior it is important to observe the Bohmian trajectory of a , for the present model, plotted in the left side of Figure 12. a , Figure 12, is plotted during the same time interval of Q , Figure 15, and its initial condition $a(\tau)$ at $\tau = 0$, was obtained from the calculation of the expected value of a , for the same model.

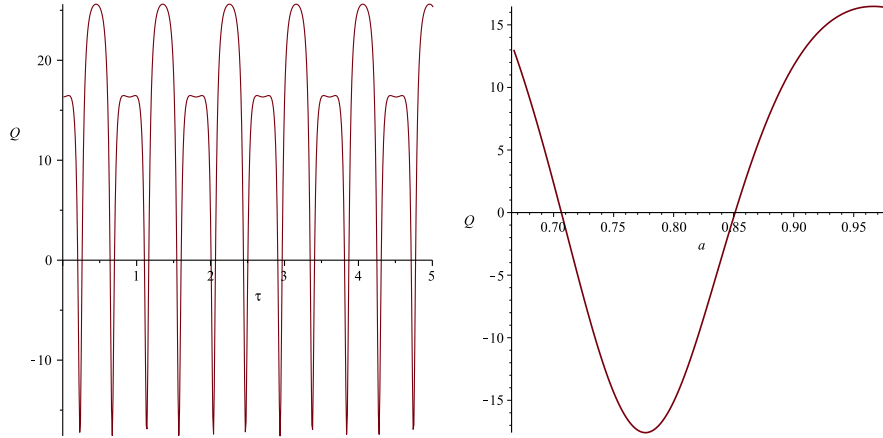


Figure 15: In the left figure, we show the quantum potential Q as a function of the time τ . In the right figure, we show the quantum potential Q as a function of the scale factor a . For both figures, the model has the following values of parameters: $g_\Lambda = -1$, $N = 2$, $g_c = 10$, $g_r = 120$ and $g_s = -2$. The Q shown above, corresponds to the Bohmian trajectory of a presented in left side of Figure 12.

5 Conclusions

In the present paper, we canonically quantized an homogeneous and isotropic Hořava-Lifshitz cosmological model, with constant positive spatial sections and coupled to radiation. We considered the projectable version of that gravitational theory without the detailed balance condition. We used the ADM formalism to write the gravitational hamiltonian of the model and the Schutz variational formalism to write the perfect fluid hamiltonian. We found the Wheeler-DeWitt equation for the model. That equation depends on several parameters coming from the HL theory. We studied the case where the values of the HL parameters are chosen, such that, the solutions to the Wheeler-DeWitt equation are bounded. Initially, we solved it using the *Many Worlds* interpretation of quantum mechanics. Using wavepackets computed with the solutions to the Wheeler-DeWitt equation, we obtained the scalar factor expected value $\langle a \rangle$. We showed that this quantity oscillates between maxima and minima values and never go to zero. That result gives an indication that the model is free from singularities, at the quantum level. We improved this result by showing that if we subtract a standard deviation of a from $\langle a \rangle$, this quantity is still positive. We, also, studied how the scale factor expected value depends on each of the HL parameters and N . Then, we used the *DeBroglie-Bohm* interpretation of quantum mechanics. First, we computed the Bohmian trajectories of a , for many different values of the HL parameters and N . We showed that a , for all those trajectories, oscillates between maxima and minima values and never go to zero, in agreement with the behavior of the expected value of a . We were, also, able to evaluate how those trajectories depend on the HL parameters and N . We compared the Bohmian trajectories of a with $\langle a \rangle$ and showed that they agree, for the corresponding models. Finally, we computed the quantum potential Q , for many different values of the HL parameters and N . We showed how that quantity helps understanding why the scale factor never vanishes, in the present HL cosmological model.

Acknowledgments

L. G. Martins thanks CAPES for her scholarship.

References

- [1] B. P. Abbott et al., Phys. Rev. Lett. **116**, 061102 (2016).
- [2] For a complete list of references see: S. W. Hawking and G. F. R. Ellis, The large scale structure of space-time, (Cambridge University Press, Cambridge, 1973).
- [3] For an introduction to this subject see: S. Weinberg, in *General Relativity. An Einstein Centenary Survey*, edited by S. W. Hawking and W. Israel (Cambridge University Press, Cambridge, 1980).
- [4] K. S. Stelle, Phys. Rev. D **16**, 953 (1977).
- [5] P. Hořava, Phys. Rev. D **79**, 084008 (2009).
- [6] S. K. Ma, Modern Theory of Critical Phenomena, (Benjamin, New York, 1976).
- [7] P. C. Hohenberg and B. I. Halperin, Rev. Mod. Phys. **49**, 435 (1977).
- [8] S. Sachdev, Quantum Phase Transitions (Cambridge University Press, Cambridge, U.K., 1999).
- [9] E. Ardonne, P. Fendley and E. Fradkin, Ann. Phys. (N. Y.) **310**, 493 (2004).
- [10] R. Arnowitt, S. Deser and C. W. Misner, in *Gravitation: an introduction to current research*, ed. L. Witten (Wiley, New York, 1962), Chapter 7, pp 227-264 and arXiv:gr-qc/0405109.
- [11] D. Blas, O. Pujolas and S. Sibiryakov, *Consistent extension of Hořava gravity*, Phys. Rev. Lett. **104**, 181302 (2010).
- [12] D. Blas, O. Pujolas and S. Sibiryakov, *On the extra mode and inconsistency of Hořava-Lifshitz*, JHEP **04**, 018 (2011).
- [13] T. P. Sotiriou, M. Visser and S. Weinfurtner, *Phenomenologically viable Lorentz-violating quantum gravity*, Phys. Rev. Lett. **102**, 251601 (2009).
- [14] T. P. Sotiriou, M. Visser and S. Weinfurtner, *Quantum gravity without Lorentz invariance*, JHEP **10**, 033 (2009).

- [15] A. Wang and R. Maartens, *Linear perturbation of cosmological models in the Hořava-Lifshitz theory of gravity without detailed balance*, Phys. Rev. D **81**, 024009 (2010).
- [16] O. Bertolami and C. A. D. Zarro, *Hořava-Lifshitz quantum cosmology*, Phys. Rev. D **84**, 044042 (2011).
- [17] J. P. M. Pitelli and A. Saa, *Quantum singularities in Hořava-Lifshitz cosmology*, Phys. Rev. D **86**, 063506 (2012).
- [18] B. Vakili and V. Kord, *Classical and quantum Hořava-Lifshitz cosmology in a minisuperspace perspective*, Gen. Relativ. Gravit. **45**, 1313 (2013).
- [19] H. Ardehali and P. Pedram, *Chaplygin gas Hořava-Lifshitz quantum cosmology*, Phys. Rev. D **93**, 043532 (2016).
- [20] Y. Misonoh, M. Fukushima and S. Miyashita, *Stability of singularity-free cosmological solutions in Hořava-Lifshitz gravity*, Phys. Rev. D **95**, 044044 (2017).
- [21] R. Maier and I. D. Soares, *Hořava-Lifshitz bouncing Bianchi IX universes: A dynamical system analysis*, Phys. Rev. D **96**, 103532 (2017).
- [22] S. F. Bramberger et al, *Solving the flatness problem with an anisotropic instanton in Hořava-Lifshitz gravity*, Phys. Rev. D **97**, 043512 (2018).
- [23] G. Oliveira-Neto, L. G. Martins, G. A. Monerat and E. V. Corrêa Silva, *De Broglie-Bohm interpretation of a Hořava-Lifshitz quantum cosmology model*, Mod. Phys. Lett. A **33**, 1850014 (2018).
- [24] A. Wang, *Hořava gravity at a Lifshitz point: A progress report*, Int. J. Mod. Phys. D **26**, 1730014 (2017).
- [25] H. Everett, *Relative state formulation of quantum mechanics*, Rev. Mod. Phys. **29**, 454 (1957).
- [26] D. Bohm and B. J. Hiley, *The undivided universe: an ontological interpretation of quantum theory*, Routledge, London, 1993;
- [27] P. R. Holland, *The quantum theory of motion: an account of the de Broglie-Bohm interpretation of quantum mechanics*, Cambridge University Press, Cambridge, 1993.

- [28] J. Acacio de Barros, N. Pinto-Neto and M. A. Sagiuro-Leal, Phys. Lett. A **241** (1998) 229.
- [29] P. Pedram and S. Jalalzadeh, Phys. Lett. B **660**, 1 (2008).
- [30] G. A. Monerat, L. G. Ferreira Filho, G. Oliveira-Neto, E. V. Corrêa Silva, C. Neves, Phys. Lett. A **374**, 4741 (2010).
- [31] B. Vakili, Phys. Lett. B **718**, 34 (2012).
- [32] S. Das, Phys. Rev. D **89**, 084068 (2014).
- [33] A. F. Ali and S. Das, Phys. Lett. B **741**, 276 (2015).
- [34] G. Oliveira-Neto, M. Silva de Oliveira, G. A. Monerat and E. V. Corrêa Silva, Int. J. Mod. Phys. D **26**, 1750011 (2016).
- [35] N. Pinto-Neto and J. C. Fabris, Class. Quantum Grav. **30**, 143001 (2013).
- [36] A. G. Riess et al. Astron. J. **116**, 1009 (1998); S. Perlmutter et al., Astrophys. J. **517**, 565 (1999).
- [37] C. W. Misner, K. S. Thorne and J. A. Wheeler, *Gravitation*, (W. H. Freeman and Company, New York, 1973).
- [38] Schutz, B. F., Phys. Rev. D **2**, 2762, (1970).
- [39] Schutz, B. F., Phys. Rev. D **4**, 3559, (1971).
- [40] F.G. Alvarenga, J.C. Fabris, N.A. Lemos and G.A. Monerat, Gen. Rel. Grav. **34**, 651 (2002).
- [41] V. G. Lapchinskii and V. A. Rubakov, Theor. Math. Phys. **33**, 1076 (1977).
- [42] P. A. M. Dirac, Can. J. Math. **2**, 129 (1950); Proc. Roy. Soc. London A **249**, 326 and 333 (1958); Phys. Rev. **114**, 924 (1959).
- [43] N. A. Lemos, J. Math. Phys. **37**, 1449 (1996).
- [44] J.P. Boyd. *Chebyshev and Fourier Spectral Methods*. 2nd ed., New York, Dover (2001).

- [45] P. Pedram, M. Mirzaei, S. Jalalzadeh, S.S. Gousheh. *Gen. Rel. Grav.* **40**, 1663 (2008).
- [46] G. Oliveira-Neto, G. A. Monerat, E. V. Corrêa Silva, C. Neves and L. G. Ferreira Filho, *Int. J. Theor. Phys.* **52**, 2991 (2013).
- [47] E. V. Corrêa Silva, G. A. Monerat, G. Oliveira-Neto and L. G. Ferreira Filho, *Comput. Phys. Commun.* **185**, 380 (2014).
- [48] R. F. Aranha, I. D. Soares and E. V. Tonini, *Phys. Rev. D* **85**, 024003 (2012).
- [49] J. Celestino, H. P. de Oliveira and E. L. Rodrigues, *Phys. Rev. D* **93**, 104018 (2016).
- [50] P. C. M. Clemente and H. P. de Oliveira, *Phys. Rev. D* **96**, 024035 (2017).
- [51] W. Barreto, P. C. M. Clemente, H. P. de Oliveira and B. R. Mueller, *Phys. Rev. D* **97**, 104035 (2018).
- [52] P. L. Meyer, *Introductory Probability and Statistical Applications*, (Addison-Wesley, Reading, 1970).